# Multidomain-staggered coupling technique for Darcy–Navier Stokes multiphase flow
## An application to $CO_2$ geosequestration

Arzanfudi, Mehdi Musivand; Saeid, Sanaz; Al-Khoury, Rafid; Sluijs, Bert

**DOI**
10.1016/j.finel.2016.07.011
**Publication date**
2016
**Document Version**
Accepted author manuscript
**Published in**
Finite Elements in Analysis and Design

# Multidomain-staggered coupling technique for Darcy-Navier Stokes multiphase flow: An application to $CO_2$ Geosequestration

*Mehdi Musivand Arzanfudi*,†, Sanaz Saeid‡, Rafid Al-Khoury†, L.J. Sluys†*

*† Faculty of Civil Engineering and Geosciences, Delft University of Technology, P.O. Box 5048, 2600 GA Delft, The Netherlands*

*‡ SGS Horizon BV., Stationsplein 6, 2275 AZ Voorburg, The Netherlands*

## Abstract

This paper introduces a multidomain-staggered technique for coupling multiphase flow in a porous medium, dominated by the Darcy laminar flow, with multiphase flow in a wellbore, dominated by the Navier Stokes viscous, compressible flow. The Darcy flow in the porous medium is formulated using the averaging theory, and the Navier Stokes flow in the wellbore is formulated using the drift-flux model. The governing equations are discretized using a mixed discretization finite element scheme, in which the partition of unity finite element method, the level set method and the standard Galerkin finite element method are combined in an integrated numerical scheme. A multidomain technique is utilized to uncouple the physical system into two subdomains, coupled back by enforcing flow constraints at their interaction boundaries. The resulting system of equations is solved using an iterative staggered technique and a multiple time-stepping scheme. This combination between the multidomain technique and the staggered-multiple time-stepping technique enables the use of different mathematical and numerical formulations for the two subdomains, and facilitates the implementation of a standard finite element computer code. The proposed model is tailored to simulate sequestered $CO_2$ leakage through heterogeneous geological formation layers and abandoned wellbores. A numerical example describing different leakage scenarios is given to demonstrate the computational capability of the model. The numerical results are compared to those obtained from a commercial simulator.

**Keywords**: integrated wellbore-reservoir simulator, multidomain, staggered technique, $CO_2$ sequestration

## 1 Introduction

Coupling multiphase flow domains exhibiting significant difference in their velocity fields using standard numerical discretization schemes is computationally nuisance and can cause severe numerical oscillations. Fluid flow in porous media related to most geoscience applications is relatively slow, and the use of Darcy's law is practically valid. Whereas, fluid flow in pipes, such as wellbores, is relatively fast and can only be described using the Navier-Stokes equations, or some of their derivatives.

In reservoir engineering, the underground reservoirs can be useful and functional only if they are connected to the ground surface. The connection is usually made using wellbores, which are utilized for injection of fluids, such as water or supercritical $CO_2$, or pumping of fluids, such as geothermal water or fossil fuels. Despite this intimate link between reservoirs and wellbores, numerical simulators utilized for design and analysis of projects related to reservoir engineering, are mostly separated. The

*** Corresponding author: Mehdi Musivand Arzanfudi**
**Faculty of Civil Engineering and Geosciences, Delft University of Technology, P.O. Box 5048, 2600 GA Delft, The Netherlands. Tel.: +31 (0)15 27 88216**
**E-mail: M.MusivandArzanfudi@tudelft.nl**

main reason for this separation is the difficulty in treating the distinct fluid flow characteristics between the reservoirs and the wellbores.

In general, there are three main techniques utilized for reservoir-wellbore integration. In one technique, the wellbore is assumed to constitute a porous domain with Darcy flow (Pruess, 2004; Réveillère and Rohmer, 2011; Zeng et al. , 2011). This assumption is, in many cases, not valid, since the wellbore is in reality a hollow space filled with fluid, where, upon flowing, the Navier-Stokes flow is physically occurring. In the other technique, the wellbore and the reservoir are modeled using separate simulators, which are linked externally as a post-processing. This is the most common technique in reservoir engineering (Ebigbo et al. , 2007; Pawar et al. , 2009). In the third one, there is a full coupling between the two domains (Nordbotten et al. , 2004; Pan et al. , 2011). Yet only few simulators are of this type, and mostly, standard numerical procedures are utilized to discretize the governing equations, entailing the need for fine grids and large CPU time and capacity.

Here, we develop a coupling technique for multiphase flow in a reservoir, connected to a wellbore. The fluid in the reservoir is governed by Darcy laminar flow, and in the wellbore by Navier-Stokes viscous, compressible flow. The two subdomains are spatially and temporally coupled, using a multidomain-staggered technique. The multidomain technique is utilized to uncouple and re-couple the physical system, and the staggered technique is utilized to solve the system of equations. The physical domain is divided into two subdomains representing the reservoir (and other rock formations), and the wellbore. At the contact points between the two subdomains, constraint conditions, controlling the fluid flow between them, are enforced. This multidomain-staggered combination allows for the use of different discretization schemes for the two subdomains, and more importantly, different time integration schemes, which count for the slow fluid motion in the porous domain and the fast fluid motion in the wellbore.

The proposed model is tailored to simulate sequestered $CO_2$ leakage through heterogeneous geological formation layers and abandoned wellbores. $CO_2$ geosequestration is a technology designed to mitigate the amount of $CO_2$ emitted into the earth atmosphere in an attempt to reduce the likely greenhouse effect. Selection of an appropriate geological formation and a proper design of a $CO_2$ sequestration plant require a good assessment of the risks of leakage. Leakage of $CO_2$ to the ground surface or upper layers containing underground water is hazardous and is considered as one of the major concerns of applying this technology. There are two major $CO_2$ leakage mechanisms: leakage through geological layers, for which the theory of multiphase flow in heterogeneous layered porous medium is applicable; and leakage through faults and abandoned wellbores, for which the theory of fluid dynamics is applicable.

In an earlier work, Arzanfudi et al. (2014 and 2015) introduced two numerical models describing these two $CO_2$ leakage mechanisms. A mixed discretization scheme has been utilized to solve these two leakage mechanisms. For the first, a stationary partition of unity finite element method (PUM) was utilized to model the discontinuity between layers of different physical properties, and the standard Galerkin finite element method (SG) was utilized to model the continuous fields. For the second, the drift flux model was utilized, taking into consideration all relevant phenomena occurring along the wellbore, including advection, buoyancy, phase change, compressibility, thermal interaction, wall friction and slip between phases. In this, the level-set method (LS) was utilized to trace the movement of the $CO_2$ front, the partition of unity to model the front and the standard Galerkin to model the continuous fields. In both cases, the implementation of the mixed PUM-LS-SG discretization scheme has enabled the use of structured, fixed meshes, regardless of the complexity of the layer geometries and the fluid front movement, and resulted in an effectively mesh-independent finite element solution. In this paper, these two models will be spatially and temporally coupled. A brief description of these models is given hereafter.

## 2 Two-phase flow in a heterogeneous layered domain

The physical domain is assumed two-dimensional multilayer, rigid, isotropic, homogeneous within a layer, and isothermal with local thermal equilibrium. Two fluids can simultaneously exist in the

reservoir: a wetting phase, represented by the formation water; and a non-wetting phase, represented by the injected $CO_2$. The fluids in the reservoir are incompressible, immiscible and do not exhibit phase change.

For $CO_2$ geosequestration, these assumptions might not be accurate in the area immediately surrounding the injection point, but further away, they are valid. Typically, $CO_2$ leakage occurs via upper layers and abandoned wellbores, which are usually far from the injection point. Additionally, the $CO_2$ in the reservoir is usually in a supercritical state, which is significantly less compressible than its gas state. Moreover, the focus here is on the numerical coupling between the two domains, which can readily be applied to more detailed conceptual models.

## 2.1 Governing equations

The continuity equations of an isothermal, immiscible and incompressible flow of a wetting phase (formation water) and a non-wetting phase ($CO_2$) in a rigid porous medium domain can be expressed as:

**Wetting phase**

$$-\phi\frac{\partial S_n}{\partial t}-\nabla\cdot\left[\mathbf{k}\lambda_w\left(\nabla p_w-\rho_w\mathbf{g}\right)\right]=0 \tag{1}$$

**Non-wetting phase**

$$\phi\frac{\partial S_n}{\partial t}-\nabla\cdot\left[\mathbf{k}\lambda_n\left(\nabla p_w+\frac{dp_c}{dS_n}\nabla S_n-\rho_n\mathbf{g}\right)\right]=0 \tag{2}$$

in which $\lambda_w=k_{rw}/\mu_w$ and $\lambda_n=k_{rn}/\mu_n$ are the wetting and non-wetting phase mobility, $\mathbf{g}$ is the gravity force vector, $\rho_w$ is the wetting phase mass density, $\rho_n$ is the non-wetting phase mass density, $S_w$ is the wetting phase saturation, $S_n$ is the non-wetting phase saturation, $\phi$ is the porosity, $p_w$ is the wetting phase pressure, $p_c$ is the capillary pressure, $\mathbf{k}$ is the absolute permeability, $k_{rw}$ and $k_{rn}$ are the wetting and non-wetting phase relative permeability (functions of saturation), and $\mu_w$ and $\mu_n$ are the wetting and non-wetting phase viscosity. The capillary pressure-saturation and relative permeability-saturation are described by Brooks and Corey (1964) relationships.

## 2.2 Numerical discretization

We adopt the wetting phase pressure – non-wetting phase saturation formulation. The wetting phase pressure in Eqs. (1) and (2) is continuous across the boundaries between heterogeneous layers, but the non-wetting phase saturation (and the capillary pressure under certain conditions) exhibits a jump. The presence of these complicated physical conditions at the boundary between layers exerts severe difficulties on the numerical solution procedure. The standard Galerkin finite element method, for instance, is not capable of simulating this problem accurately, even if a fine mesh is utilized. To tackle this, we employ a mixed discretization scheme, in which we use the standard Galerkin method (SG) to discretize the continuous wetting phase pressure, and the partition of unity finite element method (PUM) (Babuška and Melenk, 1997) to discretize the discontinuity in the non-wetting phase saturation field, such that

$$p_w(\mathbf{x},t)=\mathbf{N}(\mathbf{x})\mathbf{p}_w(t) \tag{3}$$

and

$$S_n(\mathbf{x},t)=\mathbf{N}(\mathbf{x})\mathbf{S}_n(t)+\mathbf{N}^{eh}(\mathbf{x})\tilde{\mathbf{S}}_n(t) \tag{4}$$

in which $\mathbf{N}(\mathbf{x})$ is the nodal vector of shape functions, and $\mathbf{p}_w(t)$ is the nodal vector of water pressure, $\mathbf{S}_n(t)$ and $\tilde{\mathbf{S}}_n(t)$ are the conventional and extended nodal vectors of the non-wetting phase saturation, and $\mathbf{N}^{eh}(\mathbf{x})$ is an enriched shape function, defined as

$$\mathbf{N}^{eh}(\mathbf{x}) = \mathbf{N}(\mathbf{x})H(\mathbf{x}) \tag{5}$$

where $H(\mathbf{x})$ is any function that can accurately describe the jump profile of the field within the element, which contains the discontinuity. The use of the partition of unity entails decomposing the saturation field into a continuous part and a discontinuous part, where the latter is enhanced by use of a function which closely describes the nature of the jump in the field (the Heaviside function in case of a strong discontinuity, for instance).

The weighted residual method, together with the mixed discretization scheme highlighted in Eqs. (3)-(5), are utilized to solve Eqs. (1) and (2). A detailed description of the discretization procedure and the finite element matrices is given in Arzanfudi et al. (2014).

The advantage of this model is mainly two-fold. First, it is capable of accurately capturing multiphase flow fields discontinuities between layers. Second, the physical discontinuity between layers is modelled regardless of the finite element mesh. Therefore, the mesh is not restricted to be aligned with the boundary between layers, and it can be structured, geometry-independent and relatively coarse. Fig. 1 shows the possible use of a structured mesh to model a multilayer system.

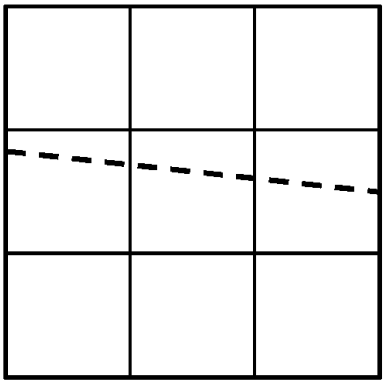

**Fig. 1. Structured and geometry-independent mesh in two-phase flow in a heterogeneous layered domain model**

## 3 Multiphase flow in a wellbore

The physical domain is assumed one-dimensional, multiphase, and constituting two compressible fluids: air and $CO_2$. The air is a homogeneous gas, and the $CO_2$ is a multiphase mixture exhibiting phase change. The physical process of such a domain is governed by the Navier-Stokes equations.

### 3.1 Governing equations

We utilize the one-dimensional drift-flux model to simulate the transport of air and $CO_2$ in the wellbore. This model adopts the area-averaged approach, where detailed analysis of the local behavior of the involved phases is averaged over the cross-sectional area of the wellbore (Faghri and Zhang, 2006; Ishii and Hibiki, 2006; Pan and Oldenburg, 2014; Wallis, 1969; Zuber and Findlay, 1965). Important aspects of fluid dynamics, such as the inertia force, buoyancy, compressibility, wall friction, drift velocity, and flow profile are considered.

The fluid velocities and pressures at the interface between the two fluids are continuous, but the mass density and specific enthalpy exhibit discontinuity, such that:

$$
\begin{aligned}
&v_{\mathrm{co}_2} = v_{\mathrm{air}} \\
&p_{\mathrm{co}_2} = p_{\mathrm{air}} \qquad\qquad \text{at}\,\Gamma_d \\
&[\![\rho_m]\!] = \rho_{\mathrm{co}_2} - \rho_{\mathrm{air}} \\
&[\![h_m]\!] = h_{\mathrm{co}_2} - h_{\mathrm{air}}
\end{aligned}
\tag{6}
$$

in which $v_{\mathrm{co}_2}$ and $v_{\mathrm{air}}$ are the velocities of $CO_2$ and air, and $h_{\mathrm{co}_2}$ and $h_{\mathrm{air}}$ are their specific enthalpies, respectively.

Taking the interface conditions, Eq. (6), into consideration, the drift-flux model is modified and expressed as:

**Mass balance**

$$
\frac{\partial \rho_m}{\partial t} + \frac{\partial}{\partial z}(\rho_m v_m) + [\![\rho_m]\!] v_m \cdot n\,\delta(z - z_d) = 0 \tag{7}
$$

**Momentum balance**

$$
\frac{\partial}{\partial t}(\rho_m v_m) + \frac{\partial}{\partial z}(\rho_m v_m^2 + \gamma) + [\![\rho_m]\!] v_m^2 \cdot n\,\delta(z - z_d) = -\frac{\partial p}{\partial z} - \frac{f\,\rho_m |v_m| v_m}{4 r_i} - \rho_m g \sin\theta \tag{8}
$$

**Energy balance**

$$
\begin{aligned}
&\frac{\partial}{\partial t}\left[\rho_m\left(h_m + \frac{1}{2}v_m^2\right) - p\right] + \frac{\partial}{\partial z}\left[\rho_m v_m\left(h_m + \frac{v_m^2}{2}\right)\right] \\
&\quad + [\![\rho_m]\!] v_m\left([\![h_m]\!] + \frac{v_m^2}{2}\right) \cdot n\,\delta(z - z_d) = \rho_m v_m g \sin\theta - \frac{Q}{\pi r_i^2}
\end{aligned}
\tag{9}
$$

where $\delta$ is the Dirac delta function, $z_d$ is the coordinate of the interface between $CO_2$ and air, $n$ is the unit normal vector (here equal to ±1), $r_i$ is the inner radius of the wellbore, $\rho_m$ is the mixture mass density, $v_m$ is the mixture velocity, $p$ is the pressure, $f$ is the wall friction coefficient, $g$ is the gravitational constant, $\theta$ is the inclination angle of the well, $h_m$ is the specific enthalpy of the mixture, $Q$ is the heat exchange between the well and its surrounding formation, and $\gamma$ describes the slip between phases.

## 3.2 Numerical discretization

We adopt the velocity – pressure – density formulation. Following Eq. (6), the velocity and pressure are continuous at the interface between $CO_2$ and air, and thus the standard Galerkin finite element method suffices, entailing

$$
v_m(z,t) = \mathbf{N}(z)\mathbf{v}_m(t) \tag{10}
$$

$$
p = \mathbf{N}(z)\mathbf{p}(t) \tag{11}
$$

in which $\mathbf{N}(z)$ is the shape functions vector, $\mathbf{v}_m(t)$ and $\mathbf{p}(t)$ are the nodal values of the mixture velocity and pressure, respectively.

On the other hand, the mass density is discontinuous at the interface between $CO_2$ and air, and for this, the partition of unity method is utilized, entailing

$$
\rho_m(z,t) = \mathbf{N}(z)\boldsymbol{\rho}_m(t) + \mathbf{N}^{eh}(z)\tilde{\boldsymbol{\rho}}_m(t) \tag{12}
$$

where $\boldsymbol{\rho}_m(t)$ and $\tilde{\boldsymbol{\rho}}_m(t)$ are the conventional and extended nodal values of the mixture density, and $\mathbf{N}^{eh}(z)$ is an enriched shape function.

The level-set method is utilized to trace the moving interface, $\Gamma_d$, between the air and the $CO_2$ zones.

The weighted residual finite element method, together with the mixed discretization scheme highlighted in Eqs. (10)-(12), are employed to solve Eqs. (7), (8) and (9). A comprehensive description of the discretization procedure and the finite element matrices are given in Arzanfudi and Al-Khoury (2015).

As for the heterogeneous layered domain model, the main advantage of this model is two-fold. First, it is capable of capturing the discontinuity between the initial fluid (air, in this case) and the leaked $CO_2$ accurately. Second, the discontinuity at the boundary between the two fluids is modelled regardless of the finite element mesh. It allows the use of a fixed, structured, and relatively coarse mesh.

## 4 Multidomain-staggered coupling scheme

As it can readily be noticed, the mathematical formulations of the fluid flow in the reservoir and the wellbore, given respectively in Sections 2 and 3, are considerably different. In the reservoir, the flow is relatively slow, dominated by Darcy flow; and in the wellbore, it is relatively fast, dominated by Navier-Stokes flow. The time scales of events in the two domains are significantly different. Accordingly, coupling them in a single domain using standard numerical discretization procedures and time integration schemes can cause numerical oscillations and requires an extensive CPU time and capacity. This may explain why most numerical simulators, which are in use in reservoir engineering, separate the two problems. Here we couple the two domains using a multidomain-staggered technique.

In solid mechanics, the multidomain mixed approximation is mainly conducted via domain decomposition and frame methods. In the first, the domain is divided into several smaller subdomains and linked together using the Lagrange multiplier, penalty method or Nitsche method (Zienkiewicz et al. , 2005). They link the subdomains via the traction (the derivative of the primary variable). The difference between the Nitche method and the other two is that it includes the Dirichlet boundary condition between the divided domains. These three techniques necessitate modifying the finite element equations. The Lagrange multiplier adds an extra degree of freedom to the finite element equations, and the penalty method and Nitsche method modify the stiffness matrix by adding a constraint parameter. The frame method, on the other hand, links the subdomains via the displacement field (primary variable) at the boundaries between them. Accordingly, the link is made via standard stiffness matrix formulation, making it more suitable for computer implementation.

In most solid mechanics applications, for which the multidomain technique is adopted, the boundaries between subdomains are homogeneous, and the displacement field is essentially continuous. In the application which we are dealing with, however, there is a Cauchy type boundary condition between the reservoir and the wellbore bottom hole, and between the wellbore and the rock formations. The first boundary condition describes the hydraulic pressure gradient between the two subdomains, and the second describes the temperature gradient. In $CO_2$ geosequestration, the hydraulic pressure gradient boundary condition is manifested by the possible leakage of $CO_2$ from the reservoir to the wellbore bottom. The pressure in both subdomains is a primary state variable. The gradient in pressure at the contact point between the reservoir and the wellbore determines the amount of $CO_2$ leakage to the wellbore. This sort of interactions makes the reservoir an external source to the wellbore, and the wellbore an external source to the reservoir. No homogeneous boundary conditions exist between them.

To solve this problem, we utilize a combination between a multidomain technique and a staggered technique. We utilize the concept of the frame method to link the two subdomains by their force vectors, and we enforce a Cauchy type constraint on their primary state variables at the boundary

between them. The resulting system of equations is solved using a staggered technique and a multiple time-stepping scheme.

The staggered technique is essentially an iterative solution method, which can be employed to solve large, coupled sets of algebraic equations. It is conducted by partitioning the equations describing the coupled state variables, usually displacement and pressure, into two (or more) sets of equations, and relating them via their force vectors. Lewis and Schrefler (2000) gave an elegant overview of the standard staggered technique and its applications. The stability of the staggered algorithm has been thoroughly discussed and addressed for a broad range of coupled field problems in several literatures, including Park et al. (1977), Park (1980), Zienkiewicz et al. (1988) and Farhat et al. (1991).

The main advantage of using the sequential iterative scheme is that it allows for the use of different spatial discretization schemes, and, importantly, different time integration schemes, which efficiently, count for the significant difference in the fluid flow velocities in the two subdomains. This entails that the finite element matrices of the two subdomains are kept intact, and only the force vectors are modified.

## 4.1 Boundary condition between reservoir and wellbore

The coupling between the reservoir and the wellbore occurs at the location where the wellbore bottom hole is connected to the reservoir. We assume that the sealing plug at the wellbore bottom hole might deteriorate with time, giving rise to a leakage path to the wellbore.

The leakage velocity at the wellbore bottom hole can be described as:

**Wetting**

$$v_w = \frac{k_p k_{rw}}{\mu_w} \frac{1}{L} (p_{w/\mathrm{Res}} - p_{\mathrm{Wel}}) \tag{13}$$

**Non-wetting**

$$v_n = \frac{k_p k_{rn}}{\mu_n} \frac{1}{L} (p_{n/\mathrm{Res}} - p_{\mathrm{Wel}}) \tag{14}$$

where $p_{n/\mathrm{Res}}$ and $p_{w/\mathrm{Res}}$ are the local reservoir $CO_2$ and water phases pressures, respectively, $p_{\mathrm{Wel}}$ is the wellbore bottom hole pressure, $k_p$ is the effective permeability of the defective cement plug, and $L$ is the thickness of the plug.

The proposed model is generic and the wellbore bottom hole pressure, $p_{\mathrm{Wel}}$, might arise from the wetting phase or the non-wetting phase. But to study the worst case scenario that might occur during $CO_2$ geosequestration, we assume that the wellbore is initially filled with air and allows only $CO_2$ to leak. The $CO_2$ in this case exhibits high advection and can rapidly reach to the top of the wellbore with large quantities.

## 4.2 Spatial Coupling

The physical domain is partitioned into two subdomains: the porous media and the wellbore. The porous media are represented by the reservoir and rock formation, where the Darcy flow is dominant; and the wellbore is represented by the borehole, where the Navier-Stokes flow is dominant. The two subdomains are coupled at the point where the wellbore and the reservoir are connected. Numerically, this implies that the wellbore acts as an external source to the reservoir, and the reservoir acts as an external source to the wellbore.

Recall the finite element system of equations of the multiphase flow in the reservoir from Arzanfudi et al. (2014). It reads:

$$
\begin{aligned}
&\begin{pmatrix} \mathbf{K}_{11} & \mathbf{K}_{12} & \mathbf{K}_{13} \\ \mathbf{K}_{21} & \mathbf{K}_{22} & \mathbf{K}_{23} \\ \mathbf{K}_{31} & \mathbf{K}_{32} & \mathbf{K}_{33} \end{pmatrix} \begin{Bmatrix} \delta\mathbf{p}_w \\ \delta\mathbf{S}_n \\ \delta\tilde{\mathbf{S}}_n \end{Bmatrix} + \begin{pmatrix} 0 & \mathbf{C}_{12} & \mathbf{C}_{13} \\ 0 & \mathbf{C}_{22} & \mathbf{C}_{23} \\ 0 & \mathbf{C}_{32} & \mathbf{C}_{32} \end{pmatrix} \begin{Bmatrix} \delta\dot{\mathbf{p}}_w \\ \delta\dot{\mathbf{S}}_n \\ \delta\dot{\tilde{\mathbf{S}}}_n \end{Bmatrix} \\
&= \begin{Bmatrix} \mathbf{f}_1 \\ \mathbf{f}_2 \\ \mathbf{f}_3 \end{Bmatrix} - \begin{pmatrix} \mathbf{K}_{11}^0 & 0 & 0 \\ \mathbf{K}_{21}^0 & \mathbf{K}_{22}^0 & \mathbf{K}_{23}^0 \\ \mathbf{K}_{31}^0 & \mathbf{K}_{32}^0 & \mathbf{K}_{33}^0 \end{pmatrix} \begin{Bmatrix} \mathbf{p}_w^r \\ \mathbf{S}_n^r \\ \tilde{\mathbf{S}}_n^r \end{Bmatrix} - \begin{pmatrix} 0 & \mathbf{C}_{12}^0 & \mathbf{C}_{13}^0 \\ 0 & \mathbf{C}_{22}^0 & \mathbf{C}_{23}^0 \\ 0 & \mathbf{C}_{32}^0 & \mathbf{C}_{33}^0 \end{pmatrix} \begin{Bmatrix} \dot{\mathbf{p}}_w^r \\ \dot{\mathbf{S}}_n^r \\ \dot{\tilde{\mathbf{S}}}_n^r \end{Bmatrix}
\end{aligned}
\tag{15}
$$

where $\mathbf{p}_w$ is the nodal vector of the wetting phase pressure; $\mathbf{S}_n$ is the nodal vector of the non-wetting phase saturation, which exhibits a jump at the boundary between layers of different physical properties, as outlined in Eq. (4); (~) represents the extended degrees of freedom due to the partition of unity; $\delta$ is the Newton-Raphson increment; and the superscript $(\cdot)^r$ is the Newton-Raphson iteration number. The first and second matrices on the left-hand side of this equation are the stiffness and the capacitance matrices, respectively. These, together with their corresponding matrices on the right-hand side, are obtained from the mixed PUM-SG discretization, outlined in Section 2. Details of the matrices are given in Arzanfudi et al. (2014).

Similarly, recall the finite element system of equations of the multiphase flow in the wellbore from Arzanfudi and Al-Khoury (2015). It reads:

$$
\begin{aligned}
&\begin{pmatrix} \mathbf{K}_{11} & 0 & \mathbf{K}_{13} & \mathbf{K}_{14} \\ \mathbf{K}_{21} & \mathbf{K}_{22} & \mathbf{K}_{23} & \mathbf{K}_{24} \\ \mathbf{K}_{31} & 0 & \mathbf{K}_{33} & \mathbf{K}_{34} \\ \mathbf{K}_{41} & 0 & \mathbf{K}_{43} & \mathbf{K}_{44} \end{pmatrix} \begin{Bmatrix} \delta\mathbf{v}_m \\ \delta\mathbf{p} \\ \delta\boldsymbol{\rho}_m \\ \delta\tilde{\boldsymbol{\rho}}_m \end{Bmatrix} + \begin{pmatrix} 0 & 0 & \mathbf{C}_{13} & \mathbf{C}_{14} \\ \mathbf{C}_{21} & 0 & \mathbf{C}_{23} & \mathbf{C}_{24} \\ \mathbf{C}_{31} & \mathbf{C}_{32} & \mathbf{C}_{33} & \mathbf{C}_{34} \\ \mathbf{C}_{41} & \mathbf{C}_{42} & \mathbf{C}_{43} & \mathbf{C}_{44} \end{pmatrix} \begin{Bmatrix} \delta\dot{\mathbf{v}}_m \\ \delta\dot{\mathbf{p}} \\ \delta\dot{\boldsymbol{\rho}}_m \\ \delta\dot{\tilde{\boldsymbol{\rho}}}_m \end{Bmatrix} \\
&= \begin{Bmatrix} \mathbf{f}_1 \\ \mathbf{f}_2 \\ \mathbf{f}_3 \\ \mathbf{f}_4 \end{Bmatrix} - \begin{pmatrix} \mathbf{K}_{11}^0 & 0 & 0 & 0 \\ \mathbf{K}_{21}^0 & \mathbf{K}_{22}^0 & \mathbf{K}_{23}^0 & \mathbf{K}_{24}^0 \\ \mathbf{K}_{31}^0 & 0 & \mathbf{K}_{33}^0 & \mathbf{K}_{34}^0 \\ \mathbf{K}_{41}^0 & 0 & \mathbf{K}_{43}^0 & \mathbf{K}_{44}^0 \end{pmatrix} \begin{Bmatrix} \mathbf{v}_m^r \\ \mathbf{p}^r \\ \boldsymbol{\rho}_m^r \\ \tilde{\boldsymbol{\rho}}_m^r \end{Bmatrix} - \begin{pmatrix} 0 & 0 & \mathbf{C}_{13}^0 & \mathbf{C}_{14}^0 \\ \mathbf{C}_{21}^0 & 0 & \mathbf{C}_{23}^0 & \mathbf{C}_{24}^0 \\ \mathbf{C}_{31}^0 & \mathbf{C}_{32}^0 & \mathbf{C}_{33}^0 & \mathbf{C}_{34}^0 \\ \mathbf{C}_{41}^0 & \mathbf{C}_{42}^0 & \mathbf{C}_{43}^0 & \mathbf{C}_{44}^0 \end{pmatrix} \begin{Bmatrix} \dot{\mathbf{v}}_m^r \\ \dot{\mathbf{p}}^r \\ \dot{\boldsymbol{\rho}}_m^r \\ \dot{\tilde{\boldsymbol{\rho}}}_m^r \end{Bmatrix}
\end{aligned}
\tag{16}
$$

where $\mathbf{v}_m$ is the nodal velocity vector of the mixture ($CO_2$ in our case), $\mathbf{p}$ is the nodal pressure vector of the mixture, and $\boldsymbol{\rho}_m$ is the nodal mass density vector, which exhibits a jump at the boundary between air and $CO_2$, as outlined in Eq. (12). The first and second matrices on the left-hand side of this equation are the stiffness and the capacitance matrices, respectively. These, together with their corresponding matrices on the right-hand side, are obtained from the mixed PUM-LS-SG discretization, outlined in Section 3. Details of the matrices are given in Arzanfudi and Al-Khoury (2015).

Coupling these two equations, Eq. (15) and (16), at their source vectors, and put them in a compact form, they can be written as

$$\mathbf{K}_{\text{Res}}\delta\mathbf{X}_{\text{Res}} + \mathbf{C}_{\text{Res}}\delta\dot{\mathbf{X}}_{\text{Res}} = \mathbf{f}_{\text{Res-Wel}} + \mathbf{f}_{\text{Res}} \tag{17}$$

$$\mathbf{K}_{\text{Wel}}\delta\mathbf{Y}_{\text{Wel}} + \mathbf{C}_{\text{Wel}}\delta\dot{\mathbf{Y}}_{\text{Wel}} = \mathbf{f}_{\text{Wel-Res}} + \mathbf{f}_{\text{Wel}} \tag{18}$$

in which all matrices and vectors terms are kept intact, except that the right-hand side of the equations is augmented with $\mathbf{f}_{\text{Res-Wel}}$ and $\mathbf{f}_{\text{Wel-Res}}$, which are the coupling source vectors that include the boundary forces at the contact node/surface between the wellbore and the reservoir. They are defined as

$$\mathbf{f}_{\mathrm{Res-Wel}} = \begin{Bmatrix} \int_{\Gamma_q^{\mathrm{Coupl}}} \mathbf{N}^T v_w d\Gamma \\ \int_{\Gamma_q^{\mathrm{Coupl}}} \mathbf{N}^T v_n d\Gamma \\ \int_{\Gamma_q^{\mathrm{Coupl}}} \left(\mathbf{N}^{eh}\right)^T v_n d\Gamma \end{Bmatrix} \tag{19}$$

and

$$\mathbf{f}_{\mathrm{Wel-Res}} = \begin{Bmatrix} -\int_{\Gamma_q^{\mathrm{Coupl}}} \mathbf{N}^T \rho_{n/\mathrm{Res}} v_n d\Gamma \\ -\int_{\Gamma_q^{\mathrm{Coupl}}} \mathbf{N}^T \rho_{n/\mathrm{Res}} v_n^{\,2} d\Gamma \\ -\int_{\Gamma_q^{\mathrm{Coupl}}} \mathbf{N}^T \rho_{n/\mathrm{Res}} v_n \left(h_{n/\mathrm{Res}} + \frac{1}{2} v_n^{\,2}\right) d\Gamma \\ -\int_{\Gamma_q^{\mathrm{Coupl}}} (\mathbf{N}^{eh})^T \rho_{n/\mathrm{Res}} v_n \left(h_{n/\mathrm{Res}} + \frac{1}{2} v_n^{\,2}\right) d\Gamma \end{Bmatrix} \tag{20}$$

where $\Gamma_q^{\mathrm{Coupl}}$ is the boundary between the reservoir and the wellbore, $v_w$ and $v_n$ are the velocities of leaking water and $CO_2$, given in Eqs. (13) and (14), and $\rho_{n/\mathrm{Res}}$ and $h_{n/\mathrm{Res}}$ are the density and specific enthalpy of $CO_2$ at the reservoir, respectively. The first term in the $\mathbf{f}_{\mathrm{Res-Wel}}$ vector belongs to the conservation of mass of the wetting phase, the second belongs to the conservation of mass of the non-wetting phase and the third is the enhanced part of the non-wetting phase, obtained by applying the partition of unity method on the saturation field. Similarly, the first term in the $\mathbf{f}_{\mathrm{Wel-Res}}$ vector belongs to the conservation of mass of the non-wetting phase, the second belongs to the conservation of momentum, and the third and fourth belong to the conservation of energy obtained by applying the partition of unity method.

At the element level, and as the reservoir upper boundary with the cap layer is embedded inside the finite elements, the contact point between the wellbore bottom hole and the reservoir does not need to conform to a node. Rather on a point inside the element, shown in Fig. 2. Using standard finite element procedure, the flux in this point is distributed at the element nodes. For a 4-node 2D element, the integral over the element length in Eq. (19) is distributed over the four nodes, and the integral in Eq. (20) reduces to a point, such that

$$\mathbf{f}_{\mathrm{Res-Wel}} = \begin{Bmatrix} \sum_{i=1}^{4} N_{\mathrm{R}i} v_w \\ \sum_{i=1}^{4} N_{\mathrm{R}i} v_n \\ \sum_{i=1}^{4} N_{\mathrm{R}i}^{eh} v_n \end{Bmatrix} \tag{21}$$

and

$$\mathbf{f}_{\text{Wel-Res}} = \begin{Bmatrix} -N_{\text{W1}}\rho_{n/\text{Res}}v_n \\ -N_{\text{W1}}\rho_{n/\text{Res}}v_n^{\ 2} \\ -N_{\text{W1}}\rho_{n/\text{Res}}v_n\left(h_{n/\text{Res}} + \frac{1}{2}v_n^{\ 2}\right) \\ -N_{\text{W1}}^{eh}\rho_{n/\text{Res}}v_n\left(h_{n/\text{Res}} + \frac{1}{2}v_n^{\ 2}\right) \end{Bmatrix} \tag{22}$$

in which the subscript W1 represents the 1D wellbore bottom hole node, and R1-R4 are the 2D four nodes of the element where the coupling occurs (see Fig. 2). Consequently, the coupling is carried out without conforming with the mesh.

The coupling element shown in Fig. 2, has two overlapping functions: partitioning the heterogeneous layered domain, via the partition of unity method; and coupling the reservoir and wellbore subdomains, via the multidomain technique.

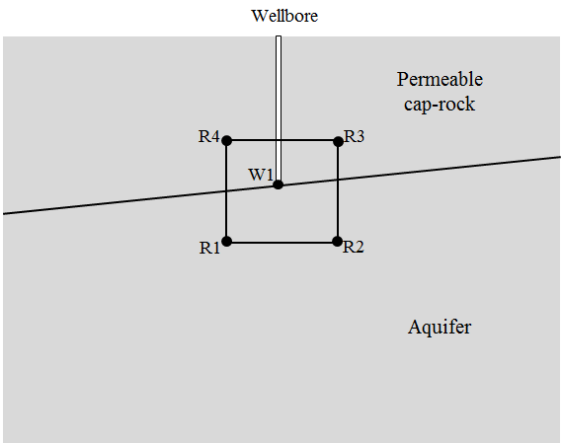


**Fig. 2 Coupling element and nodes.**

As described above, the two subdomains are coupled via their force vectors, without the use of Lagrange multiplier or penalty methods. This entails that no extra degrees of freedom or other constraint parameters are added to the finite element stiffness matrix. However, in order to enforce the constraints at the boundaries between the subdomains, a staggered solution scheme is employed.

In the staggered scheme, an iterative solution between the reservoir and the wellbore is conducted sequentially, by solving the two systems of equations independently, but updating their force vectors, Eqs. (21) and (22). The iteration continues until fulfilling the coupling condition:

$$v_n - \frac{k_p k_{rn}}{\mu_n}\frac{1}{L}(p_{n/\text{Res}} - p_{\text{Wel}}) < \varepsilon \tag{23}$$

where $\varepsilon$ is an allowable error.

Coding the staggered algorithm requires two nesting loops: an outer loop, to establish the coupling condition between the reservoir model and the wellbore model, Eq. (23); and an inner loop, for solving the reservoir and wellbore sets of equations. The simple Picard iterative scheme is sufficient to solve the resulting nonlinear scheme.

## 4.3 Temporal coupling

Sequestered $CO_2$ in saline formations is likely designed to remain in a supercritical state within the reservoir. Upon its leakage into the wellbore, the $CO_2$ is expected to undergo phase change from the

supercritical state to the gaseous state, followed by a sudden expansion due to the relatively low pressure inside the wellbore. This results in a flow regime in the wellbore that is much faster than that inside the reservoir. This entails having a significantly different time scale in the system: one in the order of months or years and another in the order of minutes or hours.

This considerable contrast in the time scale necessitates the use of different time discretization schemes. We adopt a nested multiple time integration scheme, illustrated schematically in Fig. 3. Fluid flow in the wellbore is discretized using an adaptive time step size, $\Delta t_{\mathrm{Wel}}$, which is considerably smaller than that used in the reservoir, $\Delta t_{\mathrm{Res}}$. Exchange of data between the two subsystems takes place at the end of the reservoir time step.

We utilize the $\theta$-finite difference time integration scheme to discretize Eqs. (17) and (18). Applying this scheme, for instance, on Eq. (17), yields

$$\begin{aligned}(\mathbf{C}_{\mathrm{Res}}+\theta\Delta t\mathbf{K}_{\mathrm{Res}})\delta\mathbf{X}_{\mathrm{Res}}\big|_{n+1} &= (\mathbf{C}_{\mathrm{Res}}-(1-\theta)\Delta t\mathbf{K}_{\mathrm{Res}})\delta\mathbf{X}_{\mathrm{Res}}\big|_{n} \\ &+\theta\Delta t\mathbf{f}_{\text{Res-Wel}}\big|_{n+1}+(1-\theta)\Delta t\mathbf{f}_{\text{Res-Wel}}\big|_{n}+\theta\Delta t\mathbf{f}_{\mathrm{Res}}\big|_{n+1}+(1-\theta)\Delta t\mathbf{f}_{\mathrm{Res}}\big|_{n}\end{aligned} \tag{24}$$

in which $n$ is a time step, and $0\le\theta\le1$ is the time integration parameter. The equation is solved using a standard direct solver.

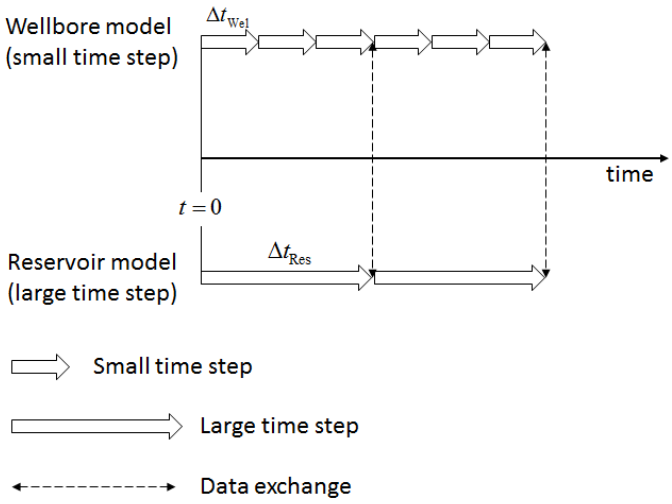


**Fig. 3 Multiple time-stepping scheme.**

Coding this multiple time-stepping scheme within the staggered solution requires an extra nested loop to take into account the small time stepping associated with the fluid flow in the wellbore. The coding algorithm is as follows:

0. Initialize $p_{\mathrm{Wel}}$ (wellbore bottom hole pressure) and $p_{n/\mathrm{Res}}$ (local $CO_2$ phase pressure at reservoir)
1. Do loop over i (reservoir time steps $\Delta t_{\mathrm{Res}}$)
2. Do loop over $v_n$
3. Initialize $v_n$ using Eq. (14)
4. Solve reservoir model, Eq. (17)
5. Calculate $p_{n/\mathrm{Res}}$
6. Do loop over j (wellbore time steps $\Delta t_{\mathrm{Wel}}$)
7. Solve wellbore model, Eq. (18)
8. End Do loop over j.

9. Calculate $p_{\mathrm{Wel}}$

10. Calculate the wellbore leakage residual error, Eq. (23). If the conditions in Eq. (23) does not hold, modify $v_n$ using Eq. (14), and go back to step 4. Otherwise exit the loop.

11. End Do loop over $v_n$.

12. Update $p_{\mathrm{Wel}}$ and $p_{n/\mathrm{Res}}$

13. End Do loop over i.

## 5 Numerical example and validation

We present a numerical example highlighting the computational capabilities of the proposed model to simulate possible leakage of sequestered $CO_2$ via the upper boundary of a reservoir and through an abandoned wellbore. Three cases describing different leakage scenarios are discussed: coupled leakage, leakage via the wellbore only, and leakage via the reservoir upper boundary only. A comparison between numerical results obtained from the proposed model and those from the Eclipse simulator (Schlumberger, 2015) is also given.

### 5.1 Coupled leakage

A $CO_2$ sequestration reservoir undergoing a possible leakage through both an upper layer and a wellbore is assumed. The conceptual geometry is shown in Fig. 4. Supercritical $CO_2$ is injected at the lower left corner of the aquifer. On the top of the aquifer, a permeable upper layer exists, with a hydraulic conductivity smaller than that of the aquifer. A leaky wellbore is intersecting the aquifer at 90 m from the injection well. The properties of the aquifer and the permeable upper layer, as well as the fluid properties are given in Table 1. The layers are initially saturated with water. The properties of the wellbore and its surrounding formation are presented in Table 2. The wellbore is initially filled with air, connected to the atmosphere at the wellbore head, and in thermodynamic equilibrium with the surrounding formation layers. The permeability of the leaky cement plug is assumed $k_p = 4 \times 10^{-13}\mathrm{m}^2$. The $CO_2$ is injected with a rate of 1.4 kg/s.

The relatively high permeability for the upper (cap) layer and the cement plug are chosen to emphasize the leakage mechanisms, which constitute the core subject of the proposed model. They represent the worst case scenarios that might occur in practice. The cap layers might be fissured due to natural causes, such as earthquakes or chemical reactions between $CO_2$ and the cap rocks. The same is valid for the wellbore sealing plug.

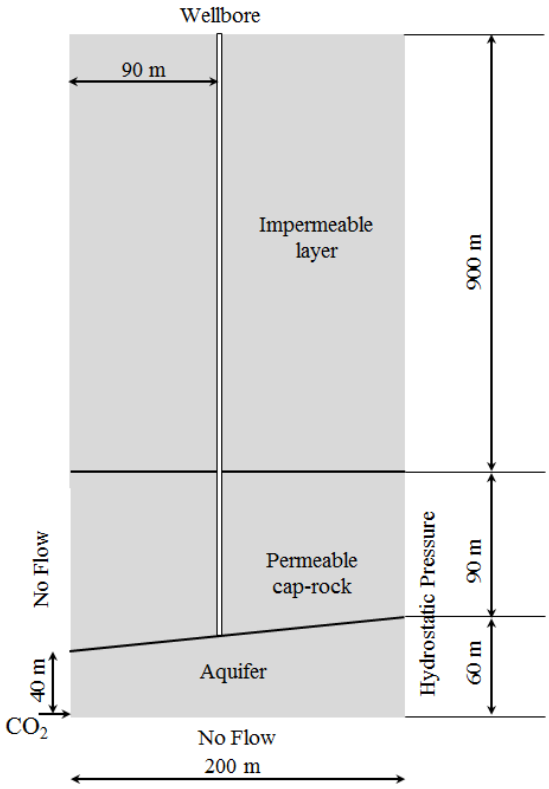


**Fig. 4 Conceptual geometry.**

**Table 1 Fluid and domain properties.**

| Fluid properties inside the reservoir | Water | $CO_2$ |
|---|---|---|
| Density [kg/m3] | 1045 | 479 |
| Viscosity [Pa.s] | $2.535\times10^{-4}$ | $3.950\times10^{-5}$ |
| Porous media properties | Aquifer (high permeable) | Upper layer (low permeable) |
| Permeability [m2] | $2.0\times10^{-12}$ | $7.5\times10^{-13}$ |
| Porosity | 0.15 | 0.1 |
| Entry pressure (Brooks-Corey ) [kPa] | 225 | 260 |
| $\hat{\theta}$ (Brooks-Corey ) | 4.0 | 2.0 |
| Water residual saturation | 0.20 | 0.20 |
| $CO_2$ residual saturation | 0.00 | 0.00 |

**Table 2 Wellbore and formation data.**

| Well Data | |
|---|---|
| Well inner radius [m] | 0.1 |
| Thickness of plug [m] | 1 |
| Heat transfer coefficient at the wellbore-formation interface ($U$ ) [W m-1 K-1] | 1.5 |
| Roughness of the wellbore [-] | $5.0\times10^{-6}$ |
| Formation Data | |
| Surface temperature [K] | 275.15 |
| Geothermal Gradient [K/m] | 0.058 |

The computational domain is illustrated in Fig. 5. The overburden top layer is not modeled; instead, the upper layer is subjected to a pressure boundary condition equivalent to the pressure exerted by the overburden layer. Four mesh sizes were utilized: 80, 204, 792 and 999 four-node elements. The wellbore is modeled using only four, two-node 1D elements. The use of this highly coarse mesh to model the fluid flow in the wellbore is only possible due to the utilization of the mixed discretization scheme to solve the wellbore governing equations (Arzanfudi and Al-Khoury, 2015).

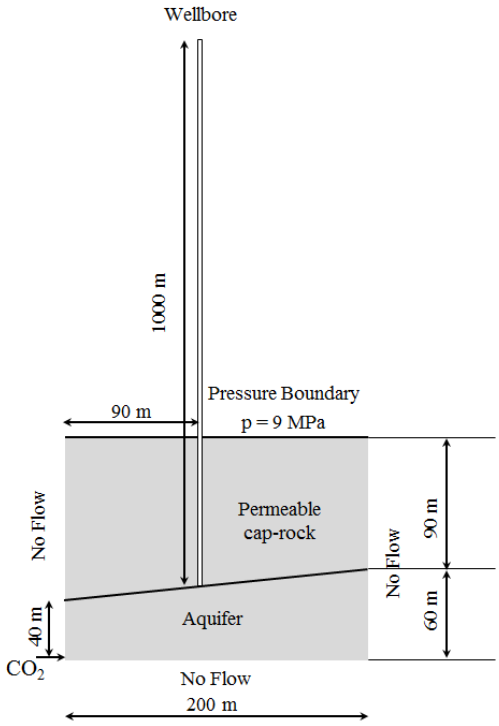


**Fig. 5 Computational domain.**

Fig. 6 shows the computed distribution of mass density, pressure, temperature and velocity along the wellbore. Despite that a very coarse mesh is utilized for the wellbore, the discontinuity in density and temperature fields between the air and the $CO_2$ is accurately captured.

Three important phenomena can be observed:

1. Once entering the wellbore, the $CO_2$ density reduces significantly, as compared to that in the reservoir,

2. with time, the $CO_2$ density starts to increase, and also

3. along the wellbore, it decreases.

Explaining these phenomena requires a closer examination of the pressure and temperature behavior along the wellbore. $CO_2$, upon entering the wellbore, expands and exhibits a significant reduction of pressure due to the Joule-Thomson effect (Green, 2008). This results into a significant reduction of density. With more leakage, the $CO_2$ accumulates at the bottom of the wellbore, leading to an increase in pressure. This gives rise to an increase in density. Along the wellbore, and due to the hydrostatic pressure, there is a reduction of pressure, accompanied by a reduction of density.

The same happens to the temperature. Upon the expansion of $CO_2$, the temperature drops significantly. But after that, and due to the second Joule-Thomson mechanism, there will be an increase in the kinetic energy of $CO_2$, which gives rise to an increase of temperature. Together with the thermal interaction with the neighboring formation, the temperature, first increases along the wellbore, and then follows a reduction trend similar to the geothermal gradient.

Regarding the velocity, at the beginning the velocity is relatively high, but due to the increase of pressure and density with time, the velocity decreases. However, along the wellbore, and due to the decrease of pressure and density, the velocity increases.

The $CO_2$ saturation fields in the reservoir and the upper layer are shown in Fig. 7 for different mesh sizes, at t = 1 day. The $CO_2$ breakthrough times, i.e. the times when the $CO_2$ starts to leak through the upper layer and through the wellbore, corresponding to the different mesh sizes, are given in Fig. 8. The amount of stored $CO_2$, as well as the amount of leaked $CO_2$ from the upper layer and the wellbore, at t = 1 day, are shown in Fig. 9. The figures show that the breakthrough times as well as the stored and leaked values computed from the 204 elements mesh give very close results to those from the finer

meshes. However, results obtained from the 80 elements mesh are reasonably accurate. This indicates that the proposed model is effectively mesh-independent, and analyses using coarse meshes are feasible.

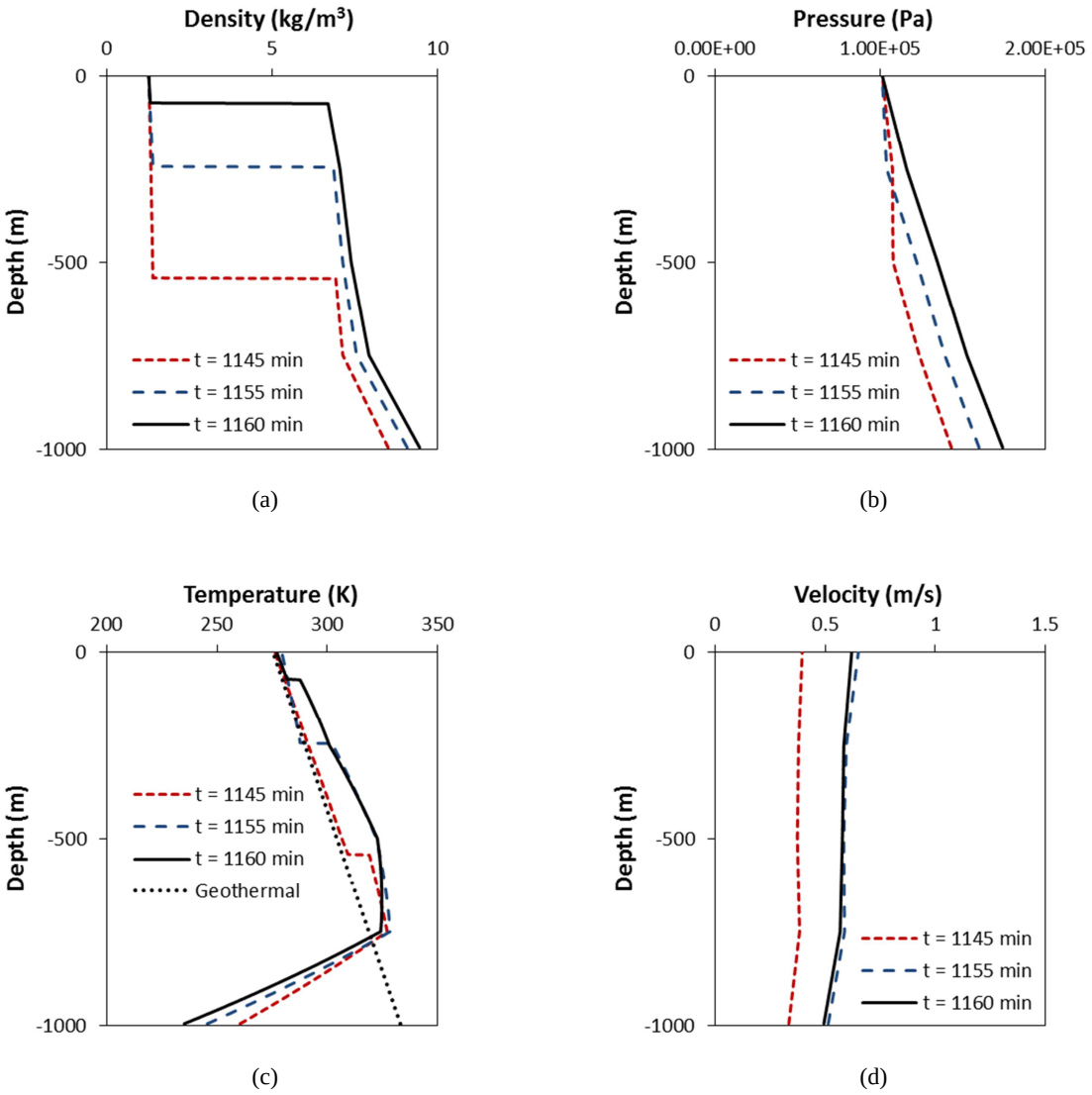


**Fig. 6 Field variables in the wellbore for the coupled leakage problem: (a) density, (b) pressure, (c) temperature, and (d) velocity.**

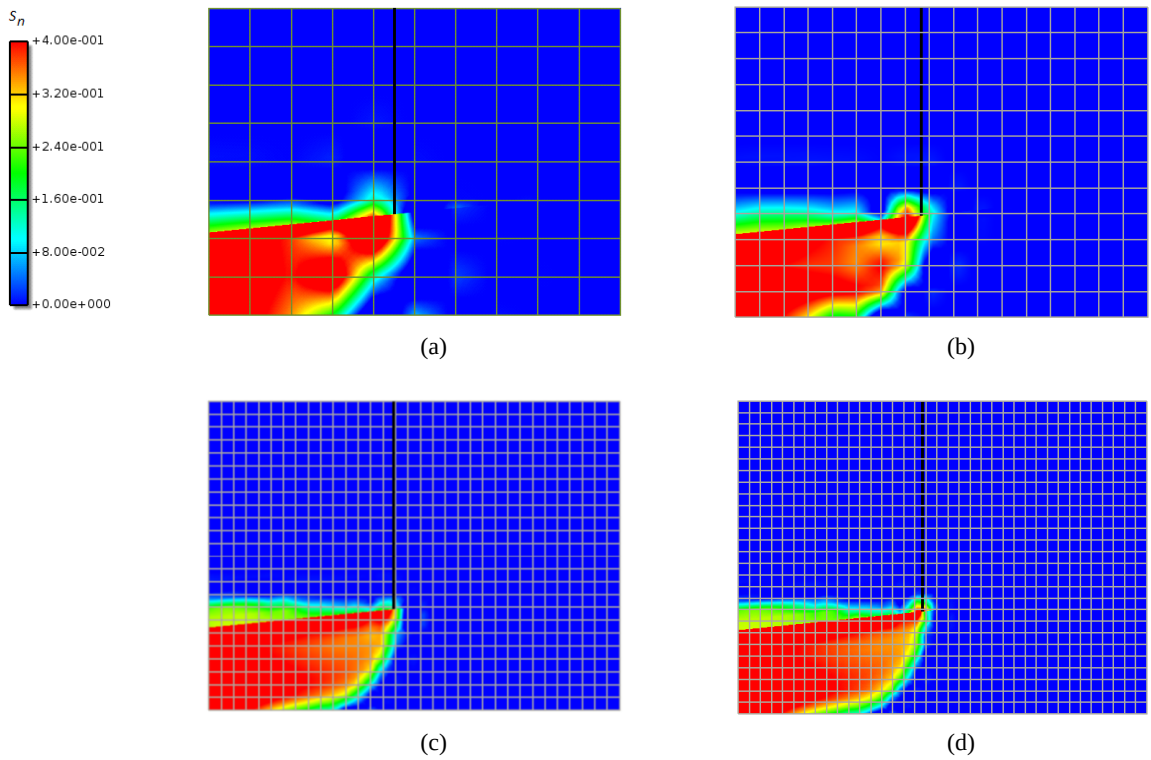


**Fig. 7 $CO_2$ saturation in the reservoir for the coupled leakage problem: (a) 80 elements, (b) 204 elements, (c) 792 elements and (d) 999 elements.**

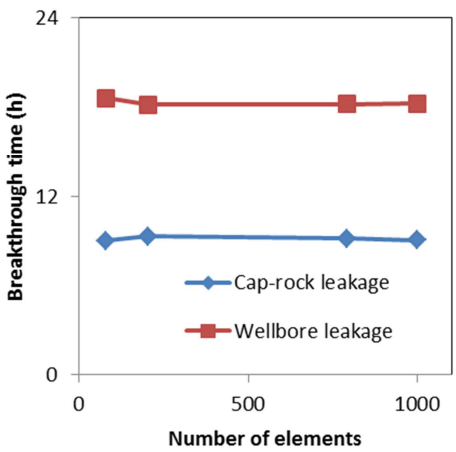


**Fig. 8 Breakthrough times for the $CO_2$ leakage start-up through the upper layer and wellbore.**

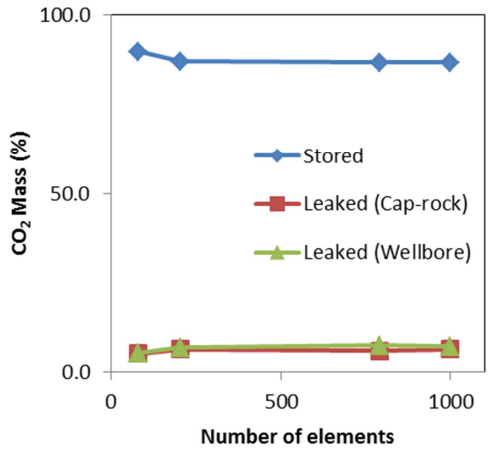


**Fig. 9 Amount of leaked and stored $CO_2$ through the cap-layer and the leaky wellbore at time t = 1 day.**

## 5.2 No layer leakage

The same problem is repeated, except that the entry pressure of the upper layer does not allow the $CO_2$ to leak from the aquifer, and the leakage can only occur through the wellbore. The same mesh sizes as for the previous example are utilized.

Fig. 10 shows the $CO_2$ saturation field in the reservoir for the different mesh sizes, at t = 1 day. The amount of stored and leaked $CO_2$ at t = 1 day are given in Fig. 11. The results again show that the stored and leaked values obtained from the analyses with the coarse meshes are close to those obtained from the finer meshes.

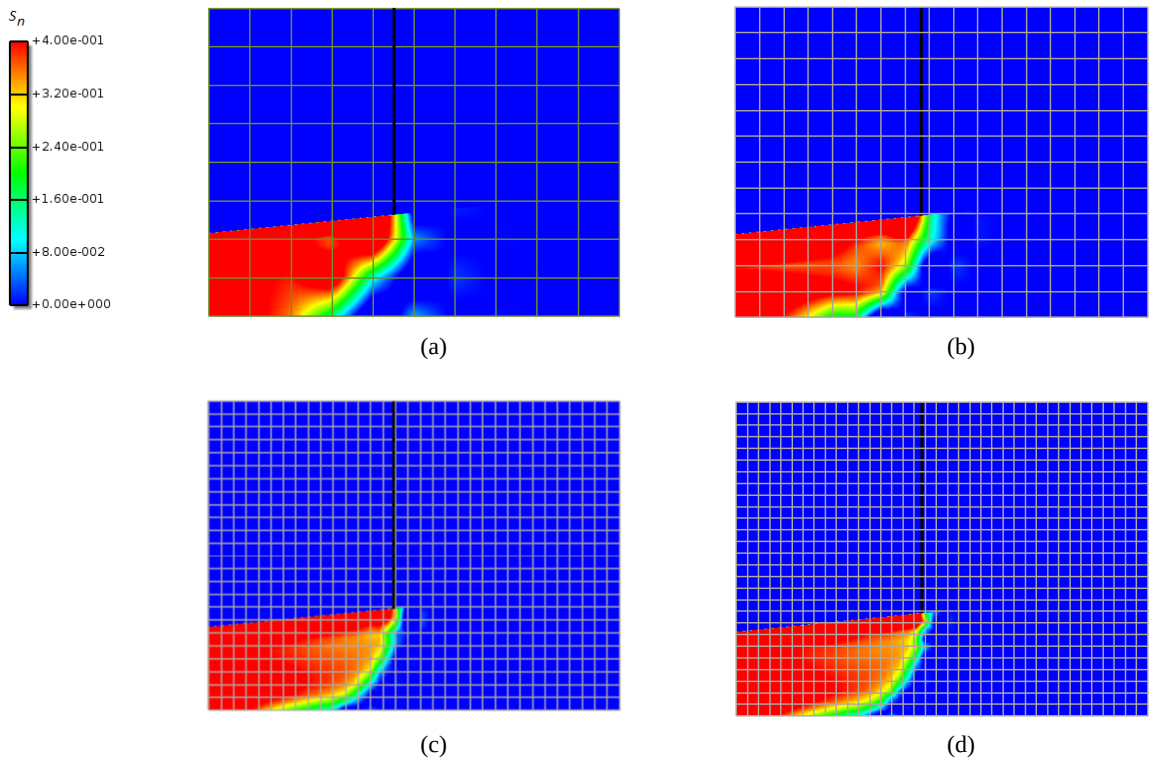


**Fig. 10 $CO_2$ saturation in the reservoir for the "no layer leakage" problem: (a) 80 elements, (b) 204 elements, (c) 792 elements and (d) 999 elements.**

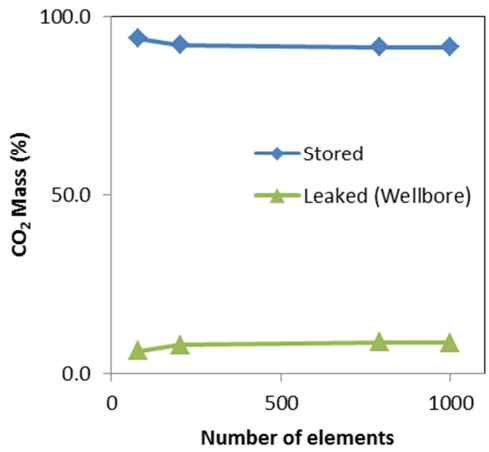


**Fig. 11 Amount of leaked and stored $CO_2$ for the "no layer leakage" problem at time t = 1 day.**

## 5.3 No wellbore leakage

A similar case is conducted, but now the leakage through the wellbore is blocked. The same mesh sizes as in the previous example are utilized.

Fig. 12 shows the $CO_2$ saturation field in the reservoir and the upper layer, for the different mesh sizes, at t = 1 day. The amount of stored and leaked $CO_2$ at t = 1 day are given in Fig. 13. The results again show that the stored and leaked values obtained from the coarse meshes are close to those obtained from the finer ones.

An interesting finding from these analyses can be deduced from the computed values of the leaked $CO_2$, as shown in Fig. 13. The amount of leakage to the upper layer occurring in the no-wellbore leakage case is more than the total amount of leakage occurring in the coupled leakage case, by a factor of 2. This can be attributed to the fact that the existence of a leaky wellbore leads to a significant change in the pressure and fluid distribution in the reservoir that eventually affect the mechanisms leading to the leakage through the upper layer. Nevertheless, leakage through the wellbore comes with a greater risk because it can rapidly reach to the surface.

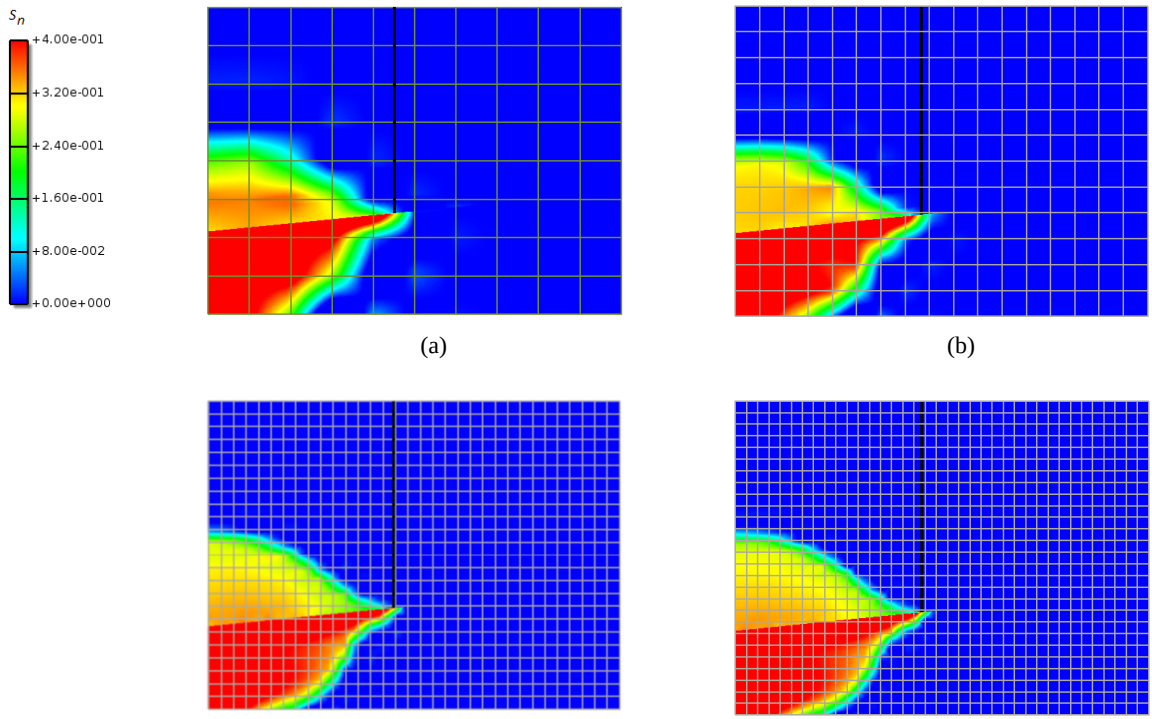


(a) (b)

(c) (d)

**Fig. 12 $CO_2$ saturation in the reservoir for the "no wellbore leakage" problem: (a) 80 elements, (b) 204 elements, (c) 792 elements and (d) 999 elements.**

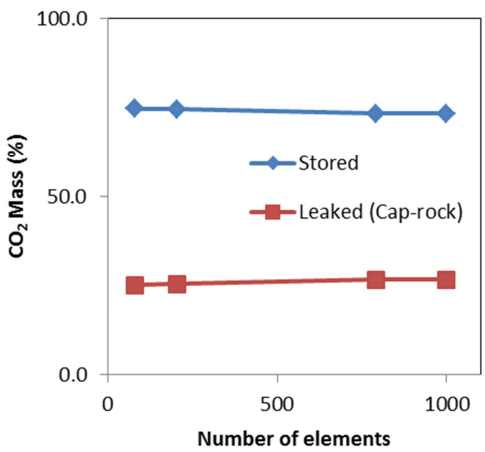


**Fig. 13 Amount of leaked and stored $CO_2$ for the "no wellbore leakage" problem at time t=1 day.**

## 5.4 Model validation

It is difficult to find in literature benchmark numerical examples including all features of the proposed model. As a consequence, we conducted a limited numerical validation comparing common computational aspects with Eclipse**,** a commercial simulator based on the finite difference method (Schlumberger, 2015). This simulator is commonly utilized for the analysis of compressible, multiphase flow in geological formations.

We compared the computational results of the three leakage scenarios, given above, with those obtained from Eclipse. However, the comparison can only be applied to the multiphase flow in the

heterogeneous porous formation. Two aspects are not possible to be compared: (i) fluid flow in the wellbore; Eclipse does not explicitly incorporate the transient fluid flow in wellbores, and (ii) compressibility in the reservoir; the proposed model assumes incompressible flow in the reservoir. To tackle these two limitations in both simulators, the numerical example is adjusted such that we make use of common features. The leakage via the wellbore in Eclipse is prescribed manually. Leakage flow rates computed by the proposed model at different time steps are imposed as a production history in Eclipse at the cell where the wellbore is connected to the reservoir. The reservoir in Eclipse is made nearly incompressible by making the variation of fluid density and viscosity, together with the formation volume factor, with pressure small.

A black oil two-phase flow model, built-in in Eclipse, is utilized for this purpose. The geometry of the reservoir and the surrounding formation, together with the initial and boundary conditions, as given in Fig. 5, are employed. The material properties and the Brook-Corey parameters are as given in Table 1.

The geometry is discretized in Eclipse using 30,000 finite difference grid cells, and in the proposed model using 999, four-node rectangular finite elements for the porous formation, and 4, two-node linear finite elements for the wellbore.

Fig. 14 shows the computational results of the three leakage scenarios computed by both simulators. The figure shows that there is a close match between the two results. The slight difference in the front shape, however, is due to the difference in the compressibility of the materials.

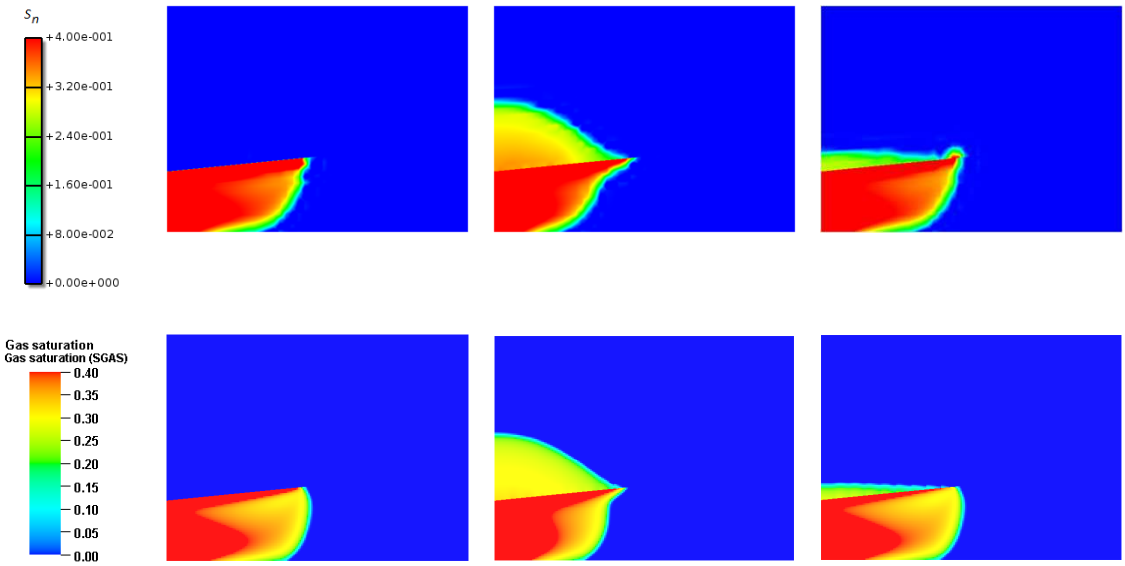


(a) (b) (c)

**Fig. 14 Comparison of computed results obtained from the proposed model (top) and Eclipse (bottom): (a) no cap-layer leakage, (b) no wellbore leakage, (c), coupled leakage**

## 6 Conclusions

In this paper we introduce a coupling technique suitable for integrating multiphase flow in a porous medium, dominated by the Darcy laminar flow; with multiphase flow in a wellbore, dominated by the Navier Stokes viscous, compressible flow. The proposed technique is tailored to simulate sequestered $CO_2$ leakage mechanisms, which might occur via abandoned wellbores and underground formations. Leakage of $CO_2$ to the ground surface or upper layers containing ground water is hazardous and considered as one of the major concerns of applying $CO_2$ sequestration technology.

As the fluid flow in the porous medium is significantly different than that in the wellbore, it is essential to design a coupling scheme, which is capable of efficiently and robustly solving the distinct mathematical formulations of the two subdomains. Here, the two subdomains are spatially and temporally coupled using a multidomain-staggered technique.

In the proposed multidomain-staggered technique, the multidomain technique is utilized to uncouple and re-couple the physical system, and the staggered technique is utilized to uncouple and solve the system of equations. The physical domain is divided into two subdomains representing the reservoir (and other rock formations), and the wellbore. At the contact points or surfaces between the two subdomains, constraint conditions are enforced. The governing equations describing the two subdomains are formulated separately, but augmented with the constraint conditions at the boundaries, where the two systems physically interact with each other. The use of the staggered technique alleviates the need for adding a Lagrange multiplier or other constraint parameters into the governing equations, normally needed in the multidomain discretization technique. Rather, the two subdomains are linked via their force (source) vector and, the boundary constraints at the contact surfaces/points are enforced iteratively. This eventually allows for the use of different time integration schemes, which count for the slow fluid motion in the porous domain and the fast fluid motion in the wellbore.

In contrast to the standard multidomain techniques, the proposed multidomain-staggered technique is essential for multiphase flow problems exhibiting significant differences in their fluid flow velocities for three main reasons:

1. It allows for the use of different mathematical and numerical formulations for the two subdomains, fostering innovative discretization schemes that can save significant computational capacity and CPU time. The computational efficiency of the proposed model is manifested by the use of structured and fixed meshes, and the gain of geometry- and effectively mesh-independent results.

2. The two subdomains are spatially coupled via their force (source) vectors, keeping their finite element matrices intact. This makes the computer implementation straightforward.

3. The two subdomains are temporally coupled using a multiple time-stepping scheme, which takes into consideration the significant difference in the fluid flow velocities. The time step of the wellbore is made small and nested in that of the reservoir.

## Acknowledgements

The authors acknowledge the financial support by AgentschapNL (Dutch Ministry of Economic Affairs) under grant number EOSLT07040. The first, third and fourth authors would also like to acknowledge the cooperation of SGS Horizon.

## References

Arzanfudi, M.M., Al-Khoury, R., 2015. A compressible two-fluid multiphase model for CO2 leakage through a wellbore. International Journal for Numerical Methods in Fluids 77: 477-507.

Arzanfudi, M.M., Al-Khoury, R., Sluys, L.J., 2014. A computational model for fluid leakage in heterogeneous layered porous media. Advances in Water Resources 73: 214-226.

Babuška, I., Melenk, J.M., 1997. The Partition of Unity Method. Int. J. Numer. Methods Eng. 40: 727-758.

Brooks, R.H., Corey, A.T., 1964. Hydraulic properties of porous media. Hydrology Paper No. 3, Colorado State Univ., Fort Collins, Colorado.

Ebigbo, A., Class, H., Helmig, R., 2007. CO2 leakage through an abandoned well: problem-oriented benchmarks. Computational Geosciences 11: 103-115.

Faghri, A., Zhang, Y., 2006. Transport phenomena in multiphase systems. Academic Press,

Farhat, C., Park, K.C., Dubois-Pelerin, Y., 1991. An unconditionally stable staggered algorithm for transient finite element analysis of coupled thermoelastic problems. Computer Methods in Applied Mechanics and Engineering 85: 349-365.

Green, D.W., 2008. Perry's chemical engineers' handbook, 8 ed. McGraw-hill, New York.

Ishii, M., Hibiki, T., 2006. Thermo-fluid dynamics of two-phase flow. 2006: Springer Science. Springer, IN, USA.

Lewis, R.W., Schrefler, B.A., 2000. The finite element method in the static and dynamic deformation and consolidation of porous media. Wiley, Chichester [u.a.].

Nordbotten, J.M., Celia, M.A., Bachu, S., Dahle, H.K., 2004. Semianalytical Solution for CO2 Leakage through an Abandoned Well. Environmental Science & Technology 39: 602-611.

Pan, L., Oldenburg, C.M., 2014. Rigorous process simulation of compressed air energy storage (CAES) in porous media systems. In: Al-Khoury, R., Bundschuh, J. (eds.) Computational Models for CO2 Geo-sequestration & Compressed Air Energy Storage. Sustainable Energy Developments, vol. 10. CRC Press, p. 574.

Pan, L., Oldenburg, C.M., Pruess, K., Wu, Y.-S., 2011. Transient CO2 leakage and injection in wellbore-reservoir systems for geologic carbon sequestration. Greenhouse Gases: Science and Technology 1: 335-350.

Park, K., Felippa, C., DeRuntz, J., 1977. Stabilization of staggered solution procedures for fluid-structure interaction analysis. Computational methods for fluid-structure interaction problems: 95-124.

Park, K.C., 1980. Partitioned Transient Analysis Procedures for Coupled-Field Problems: Stability Analysis. Journal of Applied Mechanics 47: 370-376.

Pawar, R.J., Watson, T.L., Gable, C.W., 2009. Numerical Simulation of CO2 Leakage through Abandoned Wells: Model for an Abandoned Site with Observed Gas Migration in Alberta, Canada. Energy Procedia 1: 3625-3632.

Pruess, K., 2004. Thermal Effects During CO2 Leakage from a Geologic Storage Reservoir. Lawrence Berkeley National Laboratory, http://www.escholarship.org/uc/item/5cg6209z Accessed.

Réveillère, A., Rohmer, J., 2011. Managing the risk of CO2 leakage from deep saline aquifer reservoirs through the creation of a hydraulic barrier. Energy Procedia 4: 3187-3194.

Schlumberger: ECLIPSE Simulators. http://www.software.slb.com/products/foundation/Pages/eclipse-black-oil.aspx (2015). Accessed 11 June 2015

Wallis, G.B., 1969. One-dimensional two-phase flow, vol. 1. McGraw-Hill New York,

Zeng, F., Zhao, G., Zhu, L., 2011. Detecting CO2 leakage in vertical wellbore through temperature logging. Fuel.

Zienkiewicz, O., Taylor, R., Zhu, J., 2005. The finite element method: its basis and fundamentals. Elsevier Butterworth-Heinemann, Accessed.

Zienkiewicz, O.C., Paul, D.K., Chan, A.H.C., 1988. Unconditionally stable staggered solution procedure for soil-pore fluid interaction problems. International Journal for Numerical Methods in Engineering 26: 1039-1055.

Zuber, N., Findlay, J., 1965. Average volumetric concentration in two-phase flow systems. Journal of Heat Transfer 87: 453-468.